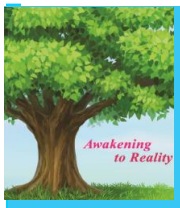

Available online at www.elixirpublishers.com (Elixir International Journal)

Thesis Publications – Mechanical Engineering

Elixir Thesis Mechanical Engineering 160TP (2020) 1-43

ISSN: 2229-712X

INFLUENCE OF JOINT DESIGN ON METALLURGICAL, CORROSION AND FATIGUE PROPERTIES OF SUBMERGED ARC WELDED AISI 316L PLATES

MASTER OF TECHNOLOGY
IN
PRODUCTION ENGINEERING

SUBMITTED BY

PANKAJ KUMAR

RAMGARHIA INSTITUTE OF ENGINEERING AND TECHNOLOGY

PHAGWARA,

PUNJAB

ARTICLE INFO

Article history:
Received: 2 September 2021;
Published: 12 November 2021;

Tele:
E-mail address: pankajkr80929@gmail.com

TABLE OF CONTENTS

LIST OF FIGURES

LIST OF TABLES

ABSTRACT

Austenitic stainless steels (ASS) represent the largest group of stainless steels and have maximum usage in industry. AISI 316L austenitic stainless steel is widely used as a structural material in chemical, petrochemical, power engineering and aviation industries owing to its good combination of mechanical properties, corrosion resistance and weldability. In view of industrial importance of this stainless steel, the proposed work would comprise of fabricating welded joints on 10mm thick AISI 316L using two different groove designs viz. Single-V groove and Narrow gap and submerged arc welding process. In view of the service applications that this alloy is subjected to, the joints will be subjected to thermal aging to high temperature of 750°C for 24 hours duration. The joints were thermally aged to study effects of precipitation at high temperature (750°C/24 hrs.) aging condition on different welds. For analyzing different aspects of these welds different specimens were extracted from the welded plates and were further subjected to metallurgical, corrosion and fatigue testing.The metallurgical testing were carried out via optical microscopy, ferrite content evaluation and microhardness measurements. Further, corrosion performance was evaluated using potentiodynamic scan for determining the pitting corrosion resistance of AISI 316L welds with different joint designs. The fatigue crack propagation behavior of different welds was determined through fatigue testing of above-mentioned welds. The results of corrosion and fatigue crack growth performance of AISI 316L welds with different joint designs and thermal aging were correlated with metallurgical observations. Mixed morphology of lacy and skeletal ferrite along with lower ferrite content and higher microhardness were observed for narrow gap butt weld as compared to single V-weld. Further, pitting corrosion resistance was also improved for joints prepared with narrow gap butt weld. The FCGR performance of narrow gap butt weld was also improved as compared to single V butt weld. Aging at high temperature reduced the pitting corrosion performance but increased the fatigue performance owing to accelerated precipitation in AISI 316L welds with different joint designs.

CHAPTER 1

INTRODUCTION

1.0 Introduction

Welding is a fabrication process that joins materials, usually metals or thermoplastics, by causing fusion, which is distinct from lower temperature metal joining techniques such as brazing and soldering, which do not melt the base metal. As per the definition given by AWS (American Welding Society), "welding is defined as a joining process producing coalescence of materials by heating them to the welding temperature, with or without the application of pressure or by the application of pressure alone, and with or without the use of fillermetal."

1.1 Submerged arc welding process

Submerged Arc Welding (SAW) involves the formation of an arc between a continuously fed electrode and the work-piece. A layer of granulated flux provides a protective shielding and a slag to protect the weld zone and may also be used to add alloying elements. The arc is submerged beneath the flux blanket that's why named submerged arc welding process.

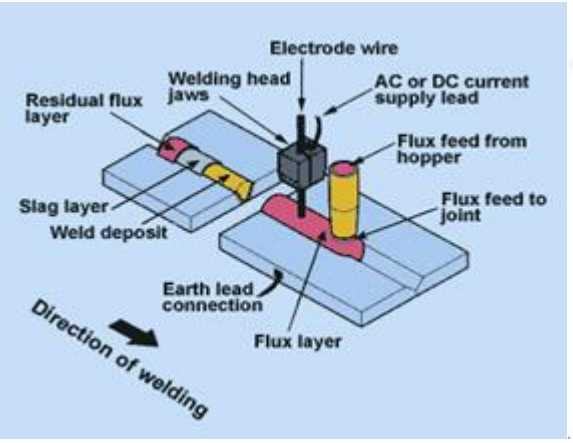

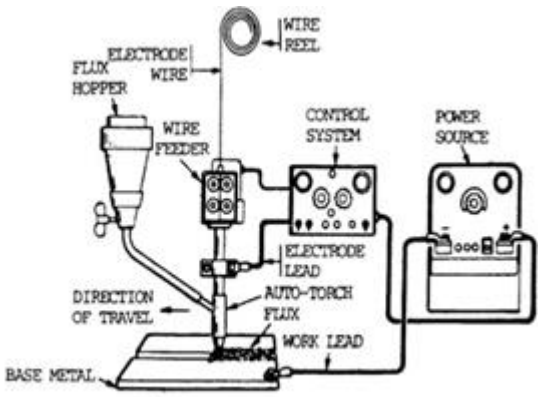

Figure 1.1. Schematic of SAW process (courtesy TWI) **Figure 1.2: Block diagram of SAW process**

The electrode may be a solid or cored wire or a strip made from sheet or sintered material. The flux may be made by either fusing constituents to form a glassy slag or by agglomerating the constituents using a binder and a corning process. The chemical nature and size distribution of the flux assists arc stability and determines the mechanical properties of the weld metal and the shape of the bead. SAW is usually operated as a mechanized process. Welding current, arc voltage and travel speed all affect bead shape, depth of penetration and chemical composition of deposited weld bead. The electrode may be a solid or cored wire or a strip made from sheet or sintered material. The flux may be made by either fusing

constituents to form a glassy slag or by agglomerating the constituents using a binder and a corning process. The chemical nature and size distribution of the flux assists arc stability and determines the mechanical properties of the weld metal and the shape of the bead. SAW is usually operated as a mechanized process. Welding current, arc voltage and travel speed all affect bead shape, depth of penetration and chemical composition of deposited weld bead.

1.2 Advantages of SAW Process

• High deposition rates.

• Molten flux provides very suitable conditions for high current to flow. Great intensities of heat can be generated and kept concentrated to weld thicker sections with deep penetration.

• High operating factor in mechanized application.

• Minimal welding fumes and arc light is emitted.

• Because of high heat concentration, considerably higher welding speeds can be used.

• Very neat appearance and smooth weld shapes can be obtained.

• The submerged arc welding process can be used for welding in exposed areas with relatively high wind.

• Welding is carried out without sparks, smoke, flash or spatter.

• Weld metal deposited possesses uniformity, good ductility and good impact strength.

1.3 Disadvantages of SAW Process

• Limited to ferrous (steel and stainless steel) and some nickel based alloys.

• Since the operator cannot see the welding being carried out, he cannot judge accurately the progress of welding.

• The flux needs pre-placing of the same on the joint which is not always possible.

• Flux and slag residue can present health and safety concern.

• The process is limited to welding in flat position and on metal more than 4.8 mm thick. In small thickness burn through is likely to occur.

• Require inter-pass and post weld slag removal.

• Requires relatively troublesome flux handling system.

• Cast iron, aluminium alloys, lead, magnesium alloys and zinc cannot be welded.

1.4 Applications

• Fabrication of pipes, pressure vessels, boilers, structural shapes, rotary kilns, rail road and earth moving equipment.

• Automotive, aviation, ship building and nuclear power industry.

- Rebuilding of worn out parts and depositing wear resisting alloys. Hard facing of tractor rollers and idlers, and crane pulleys.
- For welding mild steel, low alloy steels, stainless steels and nickel based alloys.

1.5 Austenitic Stainless steels

Austenitic stainless steels (ASS) are widely used in various applications in the chemical, petrochemical and nuclear power industries. Though resistant to uniform corrosion, austenitic stainless steels are prone to stress corrosion cracking and intergranular corrosion (localized corrosion). Elements that promote the formation of austenite such as nickel are added to these steels in large quantitites (over 8 wt. %), other strong austenite promoters carbon and nitrogen are added to some alloys to improve strength at elevated temperatures. Austenitic stainless steels generally have good toughness and ductility along with significant elongation during tensile loading. These steels have good weldability which makes them useful for manufacturing boilers and nuclear power reactors. Austenitic stainless steels include both the 200 series and 300 series alloys as designated by AISI (American Iron and Steel Institute). The 200 series alloys contain high levels of manganese, carbon and nitrogen and especially in application where galling resistance is required. The 300 series alloys are the oldest and widely used of the austenitic grades, of these commonly used types 304, 316, 321, 347 and their variants are of the 18-8 type with 18 Cr and 8-10 Ni.

1.6 Metallurgy of AISI 316 Stainless steel

The AISI 316L are molybdenum bearing austenitic stainless steel, these are usually preferred over other unstabilised ASS owing to its superior mechanical properties both at low and high temperature and higher corrosion resistance. The 2 to 3 percent molybdenum addition in these steels increases the corrosion resistance toward pitting, crevice corrosion, neutral chloride solutions and sulfurous acids. However it does not resist intergranular corrosion due to which chromium carbides formation at the adjacent matrix in the material make them sensitize in the temperature range of (550-800) 0C and hence it is not recommended for high temperature service conditions. Being extremely ductile and tough, they can be readily cold worked such as swaging, wire drawing, cold rolling etc. These steels have good welding properties and are suited to all welding procedures; they can be readily forged, hot headed and upset. SS 316 possess good creep resistance and strength along with good mechanical and corrosion properties at sub-zero temperatures. The control of carbon in SS 316L to maximum of 0.03% reduces the carbide precipitation during welding and can be used in variety of corrosive media in as welded condition.

1.7 Industrial usage of AISI 316L Stainless steel

• These steels are used in chemical containers such as to store liquid nitrogen due to its excellent toughness even down to cryogenic temperatures.

• Food industry also widely uses these steels for kitchen equipments where high chloride environments are there.

• Construction industry uses it for making structures such as railings, architectural panelling etc. Railway wagons and lines are also made with these steels due to its high mechanical properties.

• SS 316L have wide usage in boiler manufacturing industry for manufacturing boilers of high strength, corrosion and wear resistance.

• For manufacturing springs, fasteners, heat exchangers etc

• Nuclear, chemical and space industry also uses these steels in variety of applications.

1.8 Problems related to weldability of AISI 316 Stainless steel

- Sensitization.
- Pitting corrosion.
- Stress corrosion cracking.
- Fatigue failure under cyclic loading.
- Hydrogen embrittlement.

1.8.1 Pitting corrosion

Pitting is an extremely localized attack that is manifested by holes, or pits, in the metal surface. Pitting is a particularly insidious form of corrosion since it is difficult to detect until the structure has been severely attacked. Pits usually grow in the direction of gravity, only rarely forming on vertical surfaces or growing upward from the bottom of horizontal surfaces. As shown in Figure 1.3, there may be little observable damage on the surface of the structure, while in the subsurface the corrosion attack may be significant. Pitting is an autocatalytic process where by an odicmetal dissolution occurs within the pit, this anodic reaction results in the formation of an acidic (pH 1.5-2.0) solution at the bottom of the pit that results in rapid dissolution of the metal.

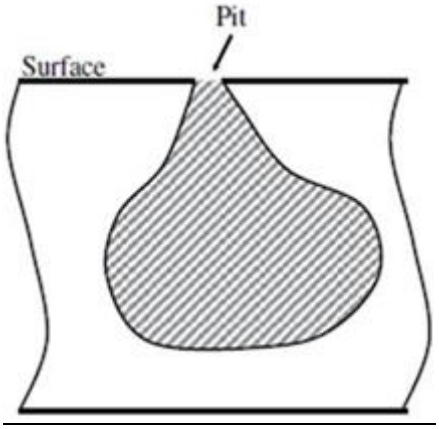

Figure 1.3. Illustration of pitting attack

1.8.2 Sensitization (Inter granular corrosion)

The problem of sensitization occurs in stainless steels in the temperature range of 550 °C to 850°C where chromium gets depleted from matrix and precipitates along the grain boundaries. The depleted chromium content reacts with carbon and leads to the formation of chromium carbide precipitates. Figure 1.4 shows the inter granular corrosion attack along the grain boundaries.

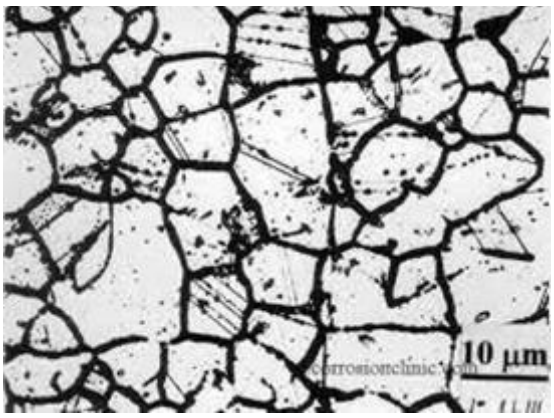

Figure 1.4. Illustration of inter granular corrosion attack

1.8.3 Stress corrosion cracking

Stress corrosion cracking (SCC) occurs when components are subjected to tensile stress in a corrosive environment. The tensile stresses may be the applied stress or the residual stresses present in the component. Figure 1.5 shows stress corrosion cracking (SCC) attack in a 316 stainless steel chemical processing piping system.

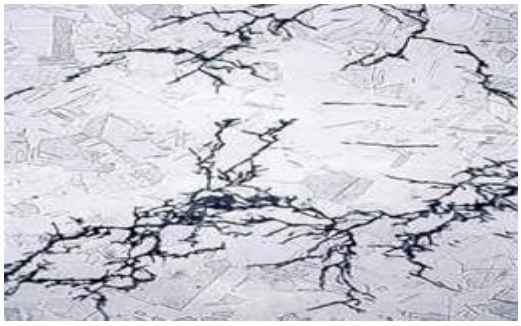

Figure 1.5. Illustration of stress corrosion cracking (SCC) attack in 316 stainless steel pipe

1.8.4 Fatigue

Fatigue is one of most common failure phenomenon related with welded fabrications. By definition, fatigue is the formation of a crack or cracks under repeated application of loads that taken individually are insufficient to cause the failure of component, that is, not of sufficient magnitude to cause plastic yielding. Fatigue is the localized and progressive structural damage that occurs when a material is subjected to cyclic loading. The nominal stress values that cause such damage may be much less than the strength of the material typically quoted as the ultimate tensile stress limit or the yield stress limit.

Since preexisting flaws and stress concentrations can be expected to occur in weldments, the service life of many welded joints is subjected to fatigue loading and component's fatigue life is dictated by crack initiation and rate of crack propagation. Since fatigue failure can occur at stresses much lower than the elastic limit (yield strength) of the material, accompanied by little or no plastic deformation with fracture progress.

Fatigue crack growth rate (da/dN) testing is designed to determine the rate of cracking under specified loading conditions once a crack has been initiated in the specimen. The graph of cyclic stress is plotted against the crack growth rate, with stress intensity being controlling variable. Fatigue crack growth rate results are reported both in tabular and graphical formats. The graphs include both da/dN vs. ΔK and crack length vs. Cycles.

1.8.5 Hydrogen embrittlement

Hydrogen embrittlement occurs in weldment owing to the presence of atomic hydrogen that results into decrease in material toughness or ductility. This type of embrittlement occurs when metals become brittle because of the diffusion of hydrogen into the material and degree of embrittlement for material is influenced by amount of hydrogen absorbed and its microstructure. Figure 1.6 shows hydrogen embrittlement.

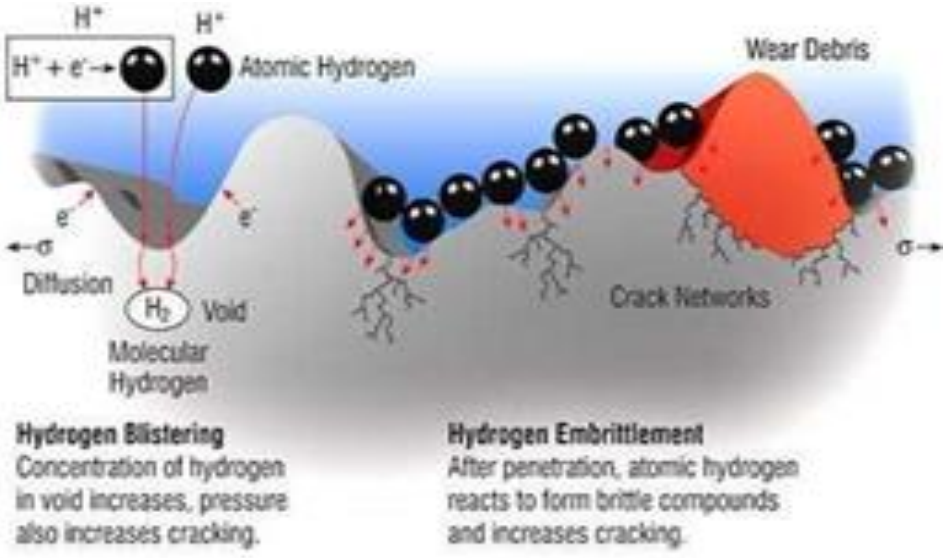

Figure 1.6. Illustration of Hydrogen embrittlement attack.

CHAPTER 2

LITERATURE REVIEW AND PROBLEM FORMULATION

2.1 Introduction

Literature review is an important part of dissertation work as it gives us the idea and direction of work. Further it helps to avoid duplication of work. Literature review helps us in the problem formulation keeping in view the research gaps, thus deciding about objectives of work. It is further important from the view point of exploring every possibility so as to extract maximum possible potential of the given material and filler wire combination. A large amount of literature is available in journals and books for AISI 316L. In this literature which directly or indirectly related to present work is discussed. Following are some of the literature worth mentioning which gave the relevant to this work.

2.2 Literature surveyed

V. Mouraet al. [1] exposed the AISI 304L to temperature range of 500-600 ℃ and concluded that weld metal was more susceptible to σ-phase (sigma-phase) formation because it contained chromium rich δ-ferrite (delta-ferrite). It was also found that base metal and weld metal were both sensitized. Healing by chromium diffusion did not happen during service. The microstructure contained inter granular chromium carbides but notσ-phase.

M. Dadfaret al. [2] studied the effect of TIG welding on corrosion behavior of AISI 316L stainles s steel. It was revealed that welding process has detrimental effect on corrosion behavior and biocompatibility of 316 L SS (stainless steel). He also found that solution heat treatment could improve the corrosion behavior of as-welded 316l SS.

M.G. Pujaret al. [3] used the induction time of passive film breakdown as a parameter to represent the pitting resistance of materials and they found that induction time was heavily dependent on the δ-ferrite content in microstructure and heat inputs of welding processes. As the heat input is increased, the induction time decreased rapidly. This was attributed to the fact that higher heat input would result in coarser δ-ferrite grains and that the passive film on the surface of coarse-grained δ-ferrite possesses low stability.

F. Liu et al. [4] investigated the creep-fatigue properties of a 308L steel weldment after different post-weld heat treatments (PWHT). PWHT promotes the creep-fatigue resistance of the weldment. The brittle sigma-phase is detrimental to the creep-fatigue resistance, PWHT enhances the creep-fatigue property of the weldment by inhibiting the precipitation of σ-

phase. The decreased precipitation ratio of σ-phase after PWHT can be attributed to relief of segregation, especially that of silicon.

U.U. KamachiMudali et al. [5] observed that the presence of sensitized microstructure at grain boundaries led to initiation and growth of pits for nitrogen bearing austenitic stainless steels. A detailed investigation on the role of sensitized microstructure indicated that pitting corrosion preceded the intergranular corrosion along the grain boundaries, as it was very sensitive to chromium depleted zones.

Rahul Unnikrishnan et al. [6] studied the effect of heat input on the microstructure, residual stresses and corrosion resistance of 304l austenitic stainless steel weldments. He concluded that ferrite content increases with increase in heat input. While hardness decreased due to increase in ferrite content of weld metal in case high heat input. Density of pitting holes increase with increase in heat input.

N. Parvathavarthini and R.K. Dayal [7] observed that carbon and chromium are the predominant compositional variables controlling sensitization kinetics. They also found that manganese reduces the carbon activity and increases its stability. Carbide precipitation is slowed down and hence it appears to inhibit carbide precipitation. Boron retards the precipitation of carbides but depending upon the heat treatment it promotes sensitization.

T.P.S. Gill et al. [8] observed that alpha prime and martensite phases formed in austenitic steels enhanced the pitting tendency due to their solubility in acidic solutions. A decrease in pitting resistance is reported for ASS welds aged at higher temperatures, and is attributed to formation of sigma and carbide precipitates. Delta ferrite in austenitic stainless steels and their weld metal also reported to be detrimental to the pitting resistance. Pitting attack was found at the delta ferrite/austenite interface, and the pits grew into austenite matrix.

MohdWarikhAbd Rashid et al. [9] investigated the formation of Cr23C6 during sensitization of AISI 304 and its effect to pitting corrosion. Study revealed that enrichment of Cr23C6 in the microstructure of AISI 304 worsens the pitting resistance as the sensitization time is increased.

CleitonCarvalho Silva et al. [10] studied the effect of welding heating cycle on AISI 316L austenitic stainless steel corrosion resistance in a medium containing Brazilian heavy petroleum. AISI 316L plates were welded using three levels of welding heat input. Thermal heat treatments were carried out at 200 and 300 ^{0}C for the period of 30 hours. Scanning electron microscopy (SEM) and analysis of X-rays dispersive energy (EDX) were used to characterize the samples. Weight loss was evaluated to determine corrosion rate. The results

show that welding heating cycle is sufficient to cause susceptibility to corrosion caused by heavy petroleum to the heat effected zone (HAZ) of the AISI 316L austenitic stainless steel.

S. Ningshen et al. [11] carried out studies in acidic chloride medium for type 304LN SS (0.086%N) and type 316LN SS (0.07% N) specimens with varying grain sizes. Specimen with different grain sizes ranging from 40 µm to 380 µm for 304L SS and from 70 µm to 570 µm for 316L SS were prepared. The studies indicated that as the grain size increased the pitting resistance deteriorated for both alloys. SEM analysis of pitted specimens revealed that at lower grain sizes, deep and stable pitting attack was seen whereas at higher grain sizes a large number of shallow pits are present. Due to large sized grains the reduction in the grain boundary area would have increased the concentration of segregated impurities. This could have weakened the passive films at such grain boundary areas leading to decrease in pitting resistance.

S.A. Tukuret al. [12] observed that ductility of sensitized specimen decreases. Sensitized specimen shows the maximum increase in strength compares to as-received and solution annealed samples. This could be attributed to the formation of a chromium carbide precipitate at the grain boundaries which restrict the dislocation movement and cause increase in yield stress of the material.

C. Graciaet al. [13] studied the four different welment zones. The results showed that HAZ was the most critical zone to intergranular corrosion for AISI 304 and 316L. The weld metal was susceptible to interdendritic corrosion and the fusion line showed the mixture of intergranular and interdendritic corrosion. The effect of pre- and post-welding heat treatments for AISI 316L was analyzed. The HAZ was again the most critical zone in every heat treatment condition.

A.I. Grekula et al [14] studied the pitting corrosion resistance of the GTAW welds with different heat inputs of AISI 316 stainless steels with 0.001% to 0.02% sulphur with phosphorous content of 0.006% using ferric chloride immersion test (ASTM G 48-76) showed that the weight loss in the primary austenitically solidifying welds (AF) was approximately $20g/m^2$ h, independent of the sulphur content, whereas the weight loss in the primary ferritically solidifying welds (FA) was markedly influenced by sulphur content. These results showed that the effect of sulphur seemed to be at its strongest just beyond the shift of solidification mode from primary austenitic to primary ferritic. It was observed that the pit density values for the welds solidified in the FA mode were higher suggesting higher pit initiation sites. This fact conclusively proved that pit initiation in weld metal was controlled by distribution impurities during solidification and the change in the mode of

solidification influenced the segregation of impurity elements across δ/γ boundaries thereby promote pitting attack at δ/γ interface.

L. Li et al. [15], studied pitting corrosion behavior of 304L austenitic stainless steels weldments joined with 308L austenitic stainless steels. Corrosion behavior of three different weldment zones weld metal (WM), base metal (BM) and heat affected zone (HAZ) was characterized by electrochemical tests. The results showed that weld metal showed a better corrosion resistance followed by heat affected zone and base metal. The pitting in base metal were much bigger than that in weld metal and heat affected zone.

Subodh Kumar and A.S. Shahi[16] investigated the influence of sensitization on the metallurgical and impact toughness behavior of GTAW AISI 304L welds. Weld metal subjected to sensitization conditions leads to carbide formation that occurs inter-dendritically along the δ-γ interface. Low heat input weld metal possess lathy ferrite morphology shows relatively low degree of sensitization (DOS) as compared to high heat input weld metal possessing vermicular ferrite morphology. As welding heat input increased, HAZ grain coarsening also increased, which resulted in higher DOS values. As post weld thermal aging time increased it resulted into higher DOS values, which significantly degrades the impact toughness of the weld metal as well as HAZ of these joints and the reason behind this behavior is carbide precipitation.

L.A. James [17] studied the fatigue-crack propagation behavior of weldments in type 304 stainless steel at 1000 ^{0}F using the technique of linear-elastic fracture mechanics. Three different welding processes were evaluated: gas tungsten arc welding (GTAW), submerged arc welding (SAW) and shielded metal arc welding (SMAW). The results revealed that the crack orientation had little effect on the crack propagation behavior of weldments produced by these processes. Study also revealed that lower growth rates are reported in weld metal and this is attributed to the duplex delta ferrite-austenite structure of the weld deposit. Apparently the many second phase particles retard crack extension.

K. Chandra et al. [18] investigated the low temperature thermal aging of austenitic stainless steel (ASS) welds. The study was conducted to analyze the ASS welds in components used in light water reactors which are susceptible to thermal aging embrittlement at reactor operating temperature of around 300 ^{0}C. Spinodal decomposition of ferrite was observed after aging which lead to embrittlement in material. The results showed that there is little effect on the tensile properties but toughness is significantly degraded after aging.

Mária Dománková et al. [19] investigated the precipitation behavior of AISI 316 in the temperature range of 500 to 900 ℃for duration of 10 minutes to 1000 hours. TTS diagrams of

experimental steel after oxalic acid etch test ASTM A262 practice were constructed. The nose of this curve was at temperature 800 ℃and time 20 minutes. Sensitization of the steel accelerated the precipitation of M23C6 carbides, besides carbide M23C6, σ-phase and carbide M6C were detected at grain boundaries. The medium size of the particles increased from 40 nm to 110 nm with increasing holding time during the heat treatment.

Ayo Afalabi et al. [20] studied the effect of heat treatment on corrosion behavior of austenitic stainless steel. The results obtained show that corrosion of all ASS samples increased with increase in tempering temperature and time. This behavior is attributed to the precipitation of chromium carbide at the grain boundaries of these metals. The metallographic images of the corroded samples showed non-uniform distribution of precipitated chromium carbide at the grain boundaries.

H. Sahlaoui et al. [21] observed that new phases will nucleate and grow in the high energy sites like grain boundaries, twin boundaries and dislocations. The study revealed that in the temperature range of 500-900 ℃ the precipitates were M23C6 carbides and they formed early in the first stage of precipitation. The intermetallic phases laves (η) (Fe2Mo) and σ (Fe-Cr) are formed after longer periods of exposure and at relatively high temperature which satisfy the kinetic and thermodynamic conditions for their nucleation and growth.

C.S. Kusko et al. [22] investigated the influence of microstructure on fatigue crack propagation behavior of gas metal arc welds in 316L and AL6XN austenitic stainless steels. The results of this test demonstrated that the large grain size of the weld metal produced a rough fracture surface with improved fatigue resistance relative to base metal. The improved fatigue resistance with increasing grain size can be attribute to a tortuous crack path that requires formation of a larger surface area for a given length of crack propagation and to crack growth out of Mode 1 plane, which reduces the stress intensity range available for crack growth.

J.J. Coronado and C. Ceron [23] analyzed the fracture mechanisms of CTOD samples of submerged and flux cored arc welding, commonly used to rebuild worn shafts in sugar cane mills. Crack tip opening displacement (CTOD) for the welds was determined according to ASTM E 1290 standard. The single deposit of FCAW process and the outer weld deposits of SAW process present acicular and blocky ferrite and non-metallic inclusions with spherical shape distributed randomly in weld in welding. The inner deposits of SAW process show equiaxed ferrite and pearlite with fine inclusions. The inner welding deposits presented highest value of CTOD as compared to outer weld deposits. The outer deposits presented

lower CTOD value, unstable crack growth and brittle fractures, characterized by intergranular failures due to fine inclusions in the grain boundaries.

Jong-Hyun Baek et al. [24] studied the fatigue crack growth rate and fracture toughness tests of type 304 stainless steel over a temperature range of -162 0C to room temperature. Girth weld metal specimens were fabricated using a combination of gas tungsten arc welding and shielded metal arc welding. The seam weld joint was made by submerged arc welding. Fracture toughness was evaluated through CTOD tests with three point bend specimens. The fatigue crack growth rate tests were conducted using compact tension specimens in accordance with ASTM E647. The CTOD values were affected by crack orientation with respect to the rolling direction, but orientation had no influence on the fatigue crack growth rate

2.3 Research Gaps

Based upon the review of the relevant literature the following research gaps were identified:

1. Literature reports on studies carried out by heat input variation and their influence on various properties of alloy AISI 316L which requires using different process parametric variations. However the influence of varying joint design has not been reported much where its influence on the metallurgical, corrosion and fatigue crack growth behavior of AISI 316L has been studied and reported.
2. Besides this for welding of 10 mm thick plates the use of narrow gap with SAW process has not been explored earlier. Further no such comparative study is reported where the use of narrow gap welds has been compared with the conventional V-groove welds.
3. Finally, AISI 316L weld joints fabricated with variable groove design have not been compared for their pitting corrosion performance, under different post weld thermal aging treatment. Further the influence of such variably precipitated welds on their fatigue performance and correlations between pitting and fatigue behavior have also not been studied earlier.

2.4 Research Objectives

In view of above mentioned research gaps the present problem was formulated with the following objectives:

1. To establish suitable welding conditions for welding 10 mm thick AISI 316L austenitic stainless steel plates using V-groove joint design and Narrow gap square butt variation leading to achieve sound quality joints.

2. To study the influence of joint design variation i.e. single-V groove and narrow gap, as well as different post weld thermal aging conditions on the metallurgical, pitting and fatigue crack growth behavior of AISI 316Lwelds.

3. To study correlations between different thermal aging conditions that influences the pitting corrosion resistance and fatigue performance of these welds.

CHAPTER 3

EXPERIMENTATION

3.1 Introduction

This chapter discusses about the procedural details that were used for used for carrying out the experimental investigations in a systematic manner so that formulated objectives of this work could be achieved, thus leading to clear and meaningful conclusions. In this chapter details regarding materials and methods are reported. The experimental procedures adopted for metallurgical behavior, fatigue and corrosion performance of welds are discussed.

3.2 Plan of experimentation

First of all trial runs were conducted to decide the welding process parameters for stainless steel welding as well as to become acquainted with the selected welding process. During trial runs both V-type and square type joints were fabricated. Specimens were cut from trial run plates to analyze the welds, so that proper side wall fusion and root fusion were obtained.

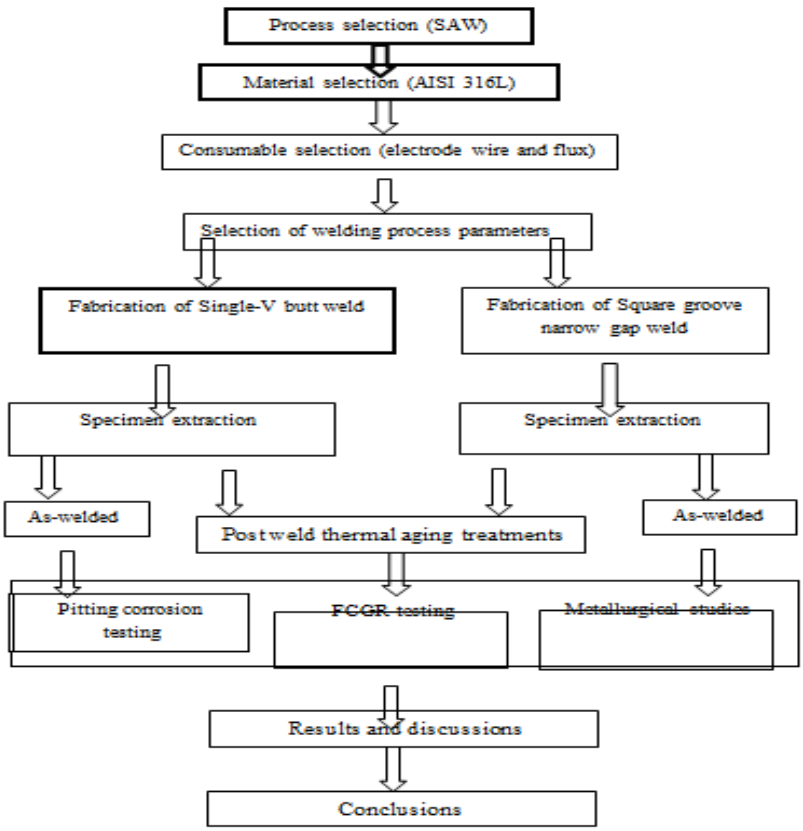

Figure 3.1. Flow chart showing methodology followed for the present work.

After the trial runs final plan was prepared and further experimentation was conducted according to the proposed plan in order to achieve the formulated objectives. The flow chart showing the sequence of steps followed to complete the work is presented on the next page.

3.3 Material Selection

Table 3.1 shows the material combination used for fabrication of welds.

Table 3.1 Material combination used for fabrication of welds

Base	AISI 316L
Filler	SAW 121 (AWS/SFA 5.9: ER 316L), Manufactured by AdorFontech Limited
Flux	AUTOMELT S33, Manufactured by Ador Welding Limited

3.3.1 Base Metal

10mm thick plates of AISI 316L were cut to required dimensions of length 500mm, width 50mm, and thickness 10mm from rolled flat. The optical emission spectroscopy (Make: Bruker) was carried out on the plate material to determine the chemical composition. The composition of the base metal is shown in Table 3.2.

Table 3.2. Chemical composition of the base metal

Element	C	Cr	Ni	Mo	Mn	S	Cu	P	Si	Fe
Weight percentage	0.027	18.89	12.35	2.56	2.00	0.03	0.35	0.045	1.00	balance

3.3.2 SAW filler wire material

SAW 121 (AWS/SFA 5.9: ER 316L) filler wire of 3.20 mm diameter was used for fabricating the joints. This filler wire usually produces austenitic stainless steel weld metal with 3 to 8% ferrite content. The composition of filler wire as per data provided by manufacturer is shown in Table 3.3.

Table 3.3. Chemical composition of filler wire

Element	C	Cr	Ni	Mo	Mn	S	Cu	P	Si	Fe
Weight percentage	0.03	18-20	11-14	2-3	1.0-2.5	0.03	0.75	0.03	0.3-0.65	balance

3.3.3 SAW Flux

AUTOMELT S33 was used for shielding the welds. The chemical composition of flux as provided by manufacturer is shown in Table 3.4.

General properties of flux are given as below:

- Agglomerated flux.
- Fluoride – basic type flux.
- High basic flux having basicity index of3.1

- Neutral behavior to carbon, so low carbon weld metal is produced with low carbon weld
- Non- chromium compensating.
- Chromium burn out is very less.
- For stainless steel.
- Suitable for welding speed of 0.4-0.6m/min.

Table 3.4. Chemical composition of AUTOMELT S33 (SAW Flux).

Element	Weight Percentage
Silicon oxide + Titanium oxide	10
Aluminum oxide + Manganese oxide	35
CaF_2	50

3.4 Welding Procedure Used

In the present work submerged arc welding (SAW) process was used for fabricating the joints. Welding procedure used for fabricating these joints is discussed as follows.

3.4.1 Pre-cleaning of baseplates

Prior to welding the first and foremost step was pre-cleaning of the base plates which involved the removal of dust or other unwanted particles from the groove edges so that defect free welds could be accomplished. The pre-cleaning was done with the help of wire brush and surface grinder so that proper fusion at the groove edges could be achieved.

3.4.2 Joint design and edge preparation

Figure 3.2 and 3.3 shows the schematic illustration of joint designs used. The joint designs used in the present work were single-V groove and Square groove with narrow gap. Single-V groove was prepared by machining on shaper by aligning of cutting head of shaper at required angle.

Single-V groove

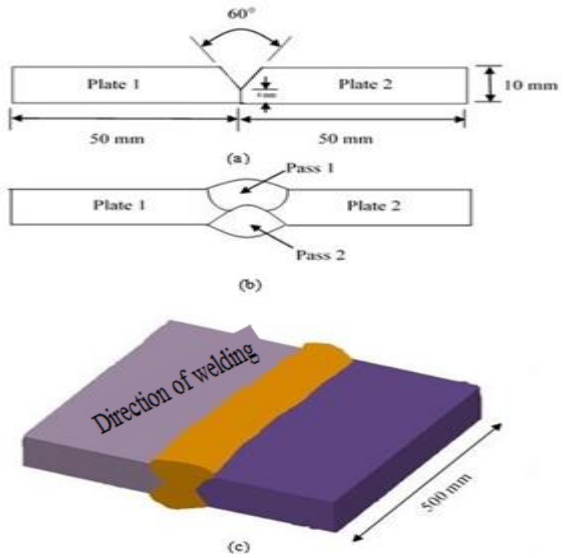

Figure 3.2. (a) Schematic illustration of plate prior to welding and joint fit-up in case of Single-V groove joint design.

(a) Schematic illustration of Single-V joint after welding.

(b) **Schematic 3-D view of fabricated Single-V joint**.

Square groove narrow gap

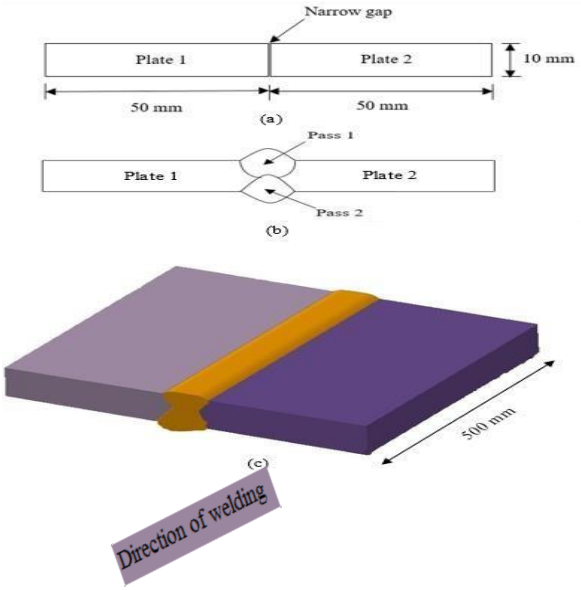

Figure 3.3. (a) Schematic illustration of plate prior to welding and joint fit-up in case of square groove narrow gap joint design.

(b) Schematic illustration of square groove narrow gap joint after welding.

(c) Schematic 3-D view of fabricated joint.

3.4.3 Welding of baseplates

Figure 3.4 shows the setup of submerged arc welding machine used for fabricating welded joints. Two process parametric combinations were finalized for fabricating Single-V groove and Square groove narrow gap joints. Table 3.5 shows the selected process parameters for fabricating the required joints. Fabrication was completed using two weld passes. First welding was done on one side and then plates are overturned to lay down the second pass. After the first weld pass back gouging was done to remove the tack welds so that proper fusion between the first and second weld pass could be obtained.

Figure 3.4. Setup of Submerged Arc Welding (SAW)

Table 3.5. Welding process parameters used in the present work.

Groove design	**Welding Current (I) Amperes**	**Voltage (V) Volts**	**Welding speed (S) mm/s**
Single-V groove joint design	475	35	7.02
Square groove narrow gap joint design	450	33	7.02

Note-1: Henceforth in the forgoing discussion Single-V groove butt weld joint has been mentioned as Single-V weld, whereas Square groove narrow gap butt weld has been mentioned as Narrow gap weld.

3.5 Specimen Cutting

Specimens for performing various studies were cut using specimen cutting machine (Make: Chennai Metco). Illustration regarding plan for specimen cutting is shown in Figure 3.5. The specimen for metallurgical and pitting studies were extracted using specimen cutting machine while compact tension C(T) sample for fatigue crack growth rate (FCGR) behavior studies were cut using electrode discharge machining process.

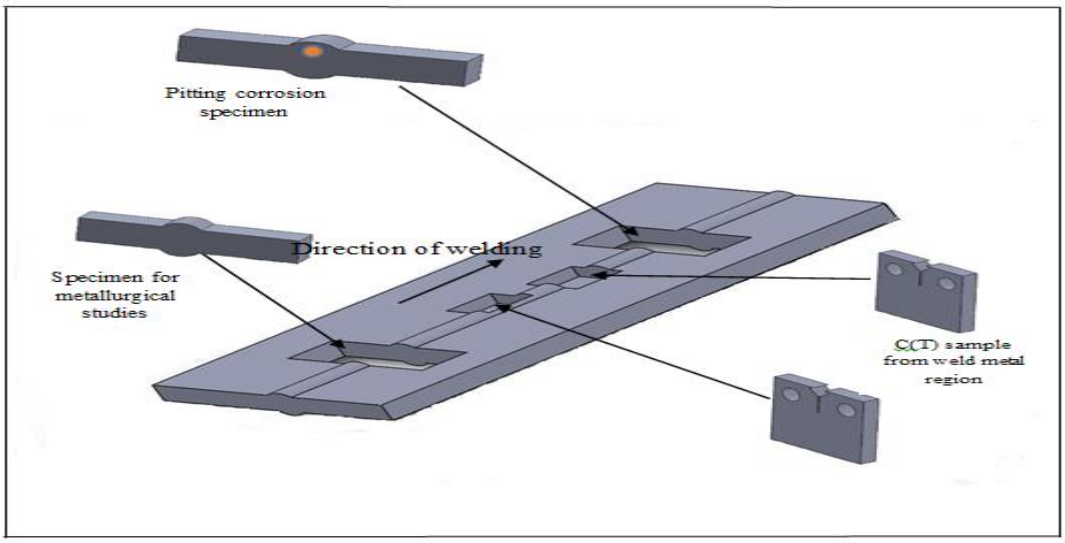

Figure 3.5. Schematic diagram showing the sampling plan from the fabricated joints

3.6 Post Weld Thermal Aging Treatment (PWTA) of extracted Samples

The samples extracted and prepared accordingly from both welded plates were thermally aged by subjecting them to varying conditions of temperature and time of exposure. The treatment conditions were selected in such a way that these thermal aging treatment led to inducing accelerated precipitation of carbides in these welds. Post weld thermal aging treatment was carried out in muffle furnace for 24 hours at 750 °C. Specimens were air cooled after aging treatment at desired conditions. The weld samples extracted for different studies from single V- weld and narrow gap weld were designated as WVT0 and WNT0 for as welded condition while WVT1 and WNT1 for samples thermally aged at 750°C for 24 hours.

Note-2: 'W' represents weld, 'V' represents Single-V weld, 'N' represents Narrow gap weld.

3.7 Pitting Corrosion Studies Using Potentio Dynamic Anodic Polarization (PAP) Technique

A Potentiostat/Galvanostat (Make: Gamry Instruments) supported by the dedicated software was used for conducting Potentiodynamic Polarization Scan on the weld sample surface to determine the pitting potential (Epit) of the welds. Figure 3.6 shows the set up for pitting corrosion studies galvanostat and paracell used for corrosion measurements. The testing was done as per recommendations of ASTM G5. The working surfaces of specimen were abraded using emery paper (Silicon carbide paper) from 100 grit size to 1000 grit size. The testing was done using paracell and the area exposed to solution in polarization scan was 0.2826 cm2 which comprised of combined zones of weldment viz. weld metal, fusion

boundary and heat affected zone (HAZ), however weld metal area was more as compared to other two zones. The electrolyte used was prepared by mixing 8.7 gram NaCl (Sodium Chloride) and 3.5 ml H2SO4 (Sulfuric acid) in 500 ml of distilled water. The solution was prepared with pure reagents. The electrode combination used in the present case comprised of graphite counter electrode, a reference electrode of saturated calomel electrode (SCE) and the working electrode (test specimen). The real time scan plots potential versus current density were recorded to evaluate the pitting corrosion behavior of the welds subjected to different thermal aging treatments.

The scan rate used was 1.67 mV/s (millivolt per second) and initial delay was for time period of 200 seconds. Potentiodynamic scan was performed from initial voltage -0.1 V vs. OCV (open circuit voltage) up to the final potential of 1.5 V vs. reference potential i.e. vs. SCE.

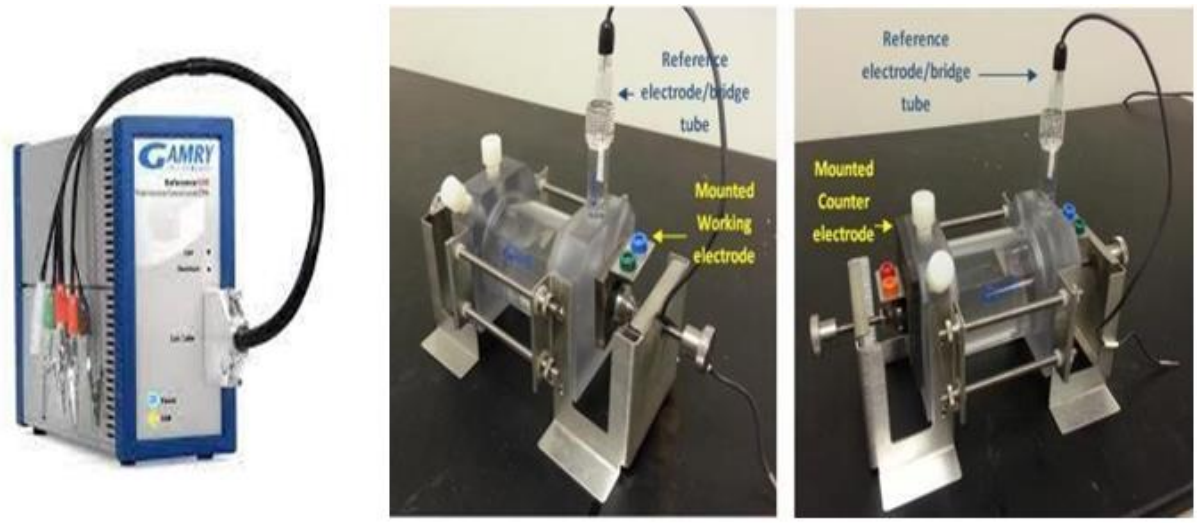

Figure 3.6. Setup for pitting corrosion studies

3.8 Metallurgical Studies of welds

To study the metallurgical effects of different joint designs and thermal aging treatments the micro hardness and microstructural studies of fabricated weldments were performed.

3.8.1 Micro hardness studies of welds

Vickers Micro hardness tester (Make: Innovatest FALCON 450) was used to measure the micro hardness variations. The samples were prepared by using emery papers starting from 100 to 1000 grit size. The polishing assisted in removing scratches and oxide layer to aid for better visualization of indents and helps in correct measurements. A load of 500 grams and dwell time of 20 seconds were used in present work. Microhardness values of weld metal in as welded condition as well as after thermal aging treatments were measured. Figure 3.7 shows the Vickers micro hardness tester.

Figure 3.7. Vickers microhardness tester.

3.8.2 Microstructural studies of welds

In order to study the effect of varying welding conditions and various thermal aging treatments the microstructural studies of specimen were conducted using inverted metallurgical optical microscope coupled with a high resolution camera and supported by dedicated software. Figure 3.8 shows the optical microscope used (Make: Olympus) for this study. The specimens were extracted from both the welded plates and also subjected to different aging treatments. The specimens used for microstructural studies were prepared with mesh grades of ASTM 100, 150, 220, 320, 400, 600, 800, 1000, 1200, 1500, 2000, 2500, 3000 and finally polished on velvet cloth using alumina paste to obtain the mirror like finish. Microstructure of weld metal zone were captured. Table 3.8 shows the chemical composition of Carpenteretchant.

Figure 3.8. Optical microscope

Table 3.6. Chemical composition of the Carpenter etchant

Compound	Quantity
Ferric chloride	8.5 gram
Cupric chloride	2.4 gram
Alcohol	122 ml
Hydrochloric acid	122 ml
Nitric acid	6 ml

3.9 Fatigue Crack Growth Rate (FCGR) Studies of welds

Fatigue crack growth behavior for AISI 316L welded plates fabricated with different joint design was evaluated using servo-hydraulically controlled fatigue testing machine (Make: Biss 50 kN capacity) as shown in Figure 3.10. FCGR behavior of samples extracted from weld metal region was evaluated in the as-welded condition as well as after thermal aging treatment. The dimensions of the CT (compact tension) sample were shown in Figure 3.9. Samples were prepared as per ASTM E1820 and E 1290. The samples were pre-cracked to 5.5 length, along the direction of welding. Extensometer is mounted to record the crack movement. The dedicated software was used to record all the data and generate required graphs for further analysis. The testing conditions for all specimens were kept constant and crack extension from 5.5 mm to 11.25 mm was analyzed for studying fatigue behavior of welded plates. Table 3.9 shows the FCGR testing conditions for compact tension C(T) sample.

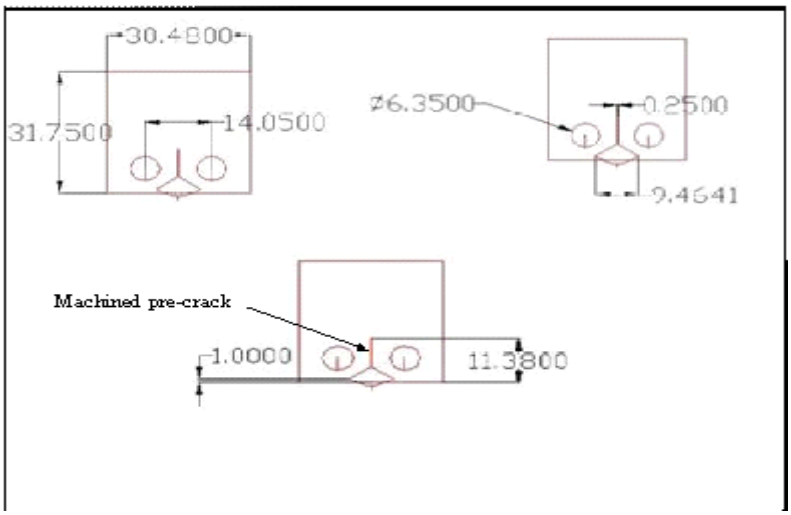

Figure 3.9. Specifications of compact tension C(T) sample showing the dimensional details.

Table 3.7. FCGR testing conditions for compact tension C(T) sample

Variable name	**Value**
Waveform	Sinusoidal meanup
Frequency	10 Hertz
Maximum load (P_{max})	6 kN
Minimum load (P_{min})	1.2 kN
Stress ratio (R)	0.2

Figure 3.10. Servo hydraulically controlled fatigue testing machine.

3.10 Ferrite content measurement

The delta ferrite content measurements were performed using non-destructive technique magnetic induction technique. As the delta ferrite content is magnetic in character, so amount of magnetic content is measured in weldments to analyze the delta ferrite content in welds. The measurements were performed using Feritscope (Make:Fischer).

CHAPTER 4

RESULTS AND DISCUSSION

4.1 Introduction

This chapter presents the experimental results obtained from metallurgical studies, pitting corrosion and Fatigue crack growth rate testing carried out on AISI 316L submerged arc welds in the as welded and thermally aged conditions. The results are presented in tabular as well as graphical form and the discussion of these results was done accordingly for welds with different joint designs.

4.2 Metallurgical studies

To study the metallurgical behavior of welds in the as deposited and thermally aged conditions, micro hardness testing and optical microscopy studies were carried out.

4.2.1 Micro hardness testing of welds

In order to study the variation in micro hardness of different welds micro hardness measurements of each weld pass in the as welded as well as after PWTA treatments were taken and results of the same are presented in Tables 4.1 and 4.2.

Micro hardness results shown in Tables 4.1 and 4.2 indicates that weld metal of the Narrow gap weld had higher micro hardness as compared to the Single-V weld, which was attributed to change in the groove designs used. Micro hardness values were higher at the weld center this could be attributed to formation of HAZ in weld pass-1. There was increase in hardness value for both the joints at high temperature aged condition of 750°C for 24 hours owing to accelerated carbides precipitation at high temperature.

Table 4.1. Microhardness results of specimens extracted from Single-V groove butt weld in the as-welded and after PWTA treatment (HV0.5).

PWTA treatments			Single-V weld		
Temperature (°)	**Time (hours)**	**Specimen code**	**Weld top surface (weld pass 1)**	**Weld center**	**Weld bottom surface (weld pass 2)**
As-welded		WVT0	177.2	195.2	174.9
750	24	WVT1	200.5	214.6	206.4

Table 4.2. Micro hardness results of specimens extracted from Narrow gap butt weld in the as- welded and after PWTA treatment (HV0.5).

PWTA treatments			Narrow gap weld		
Temperature (°C)	**Time (hours)**	**Specimen code**	**Weld top surface (weld pass 1)**	**Weld center**	**Weld bottom surface (weld pass 2)**
As-welded		WNT0	182.4	199.4	184.2
750	24	WNT1	203.5	217.3	206.5

4.2.2 Microstructural analysis of welds

Microstructural studies were carried out on the weld samples in the as-welded condition as well as at high temperature thermal aging treatment. The photomicrographs of the same are presented in Figures 4.1 to 4.4. The photomicrographs had been taken from the top cross section of the specimen.

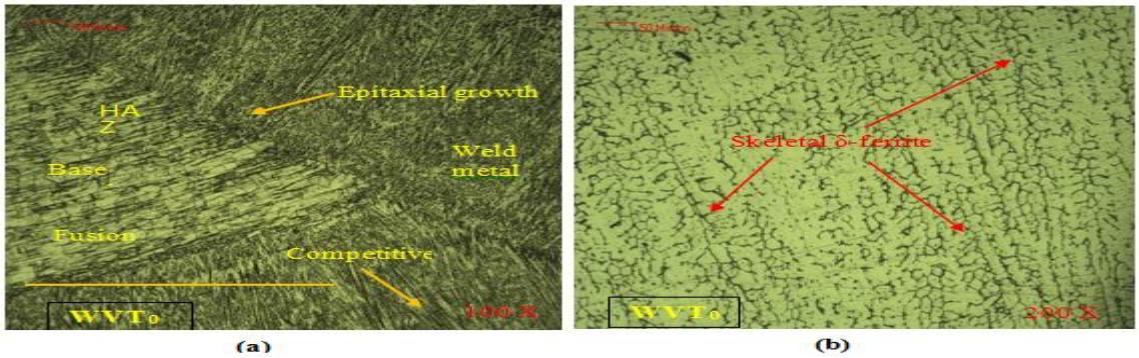

Figure 4.1.Photomicrographs of submerged arc AISI 316L Single-V weld in the as-welded condition showing (a) Different zones of weldment near weld root region (b) Skeletal δ-ferrite morphology dispersed in austenite matrix of solidified weld metal.

Figure 4.1 (a) and 4.2 (a) show different zones of weldment near the weld root region. Photomicrographs clearly showed the epitaxial growth near the fusion boundary and also the partially melted grains present on it. The existing partially melted base material grains at the fusion boundary act as a substrate for nucleation of dendrites of weld metal. Away from the fusion boundary competitive growth was observed. Also it was observed that the slope fusion boundary was less in case of Single-V weld as compared to the Narrow gap weld.

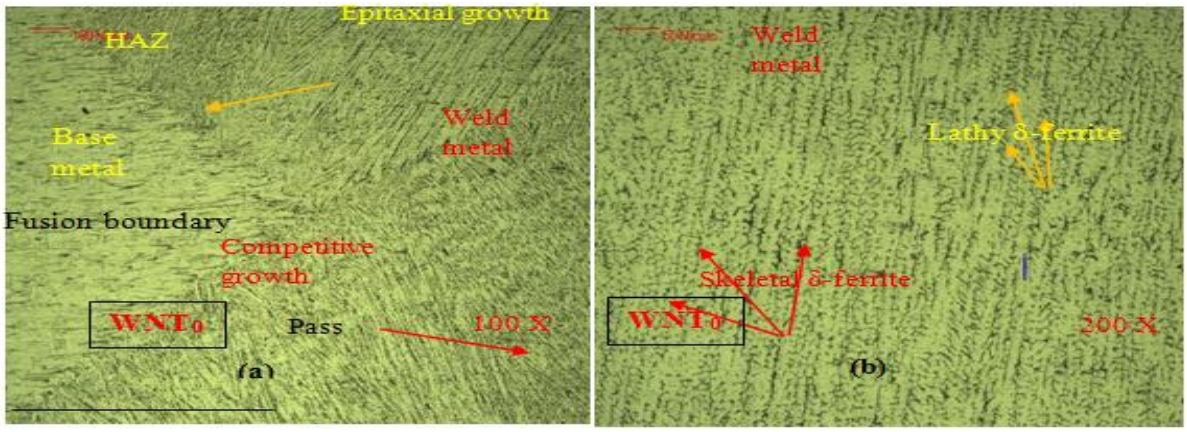

Figure 4.2. Photomicrographs of submerged arc AISI 316L Narrow gap welds in the as-welded condition showing.(a) Different zones of weldments near weld root region. (b) Skeletal and lathy δ-ferrite morphology dispersed in austenite matrix of solidified weld Metal

Figure 4.1(b) and 4.2(b) show the morphologies of δ-ferrite (delta-ferrite) in the weld metal. In case of Single-V weld (WVT0) skeletal δ-ferrite morphology was observed but in case of narrow gap weld (WNT0) both skeletal and lathy morphologies of δ-ferrite were observed. Lathy δ- ferrite was produced when austenite nucleated at ferrite grain boundaries. But if austenite nucleates in liquid as a layer around the primary ferrite dendrites then skeletal ferrite was obtained. Microstructures revealed for the welded specimens (WVT0 and WNT0) showed the presence of partially transformed ferrite dendrites dispersed in austenite matrix.

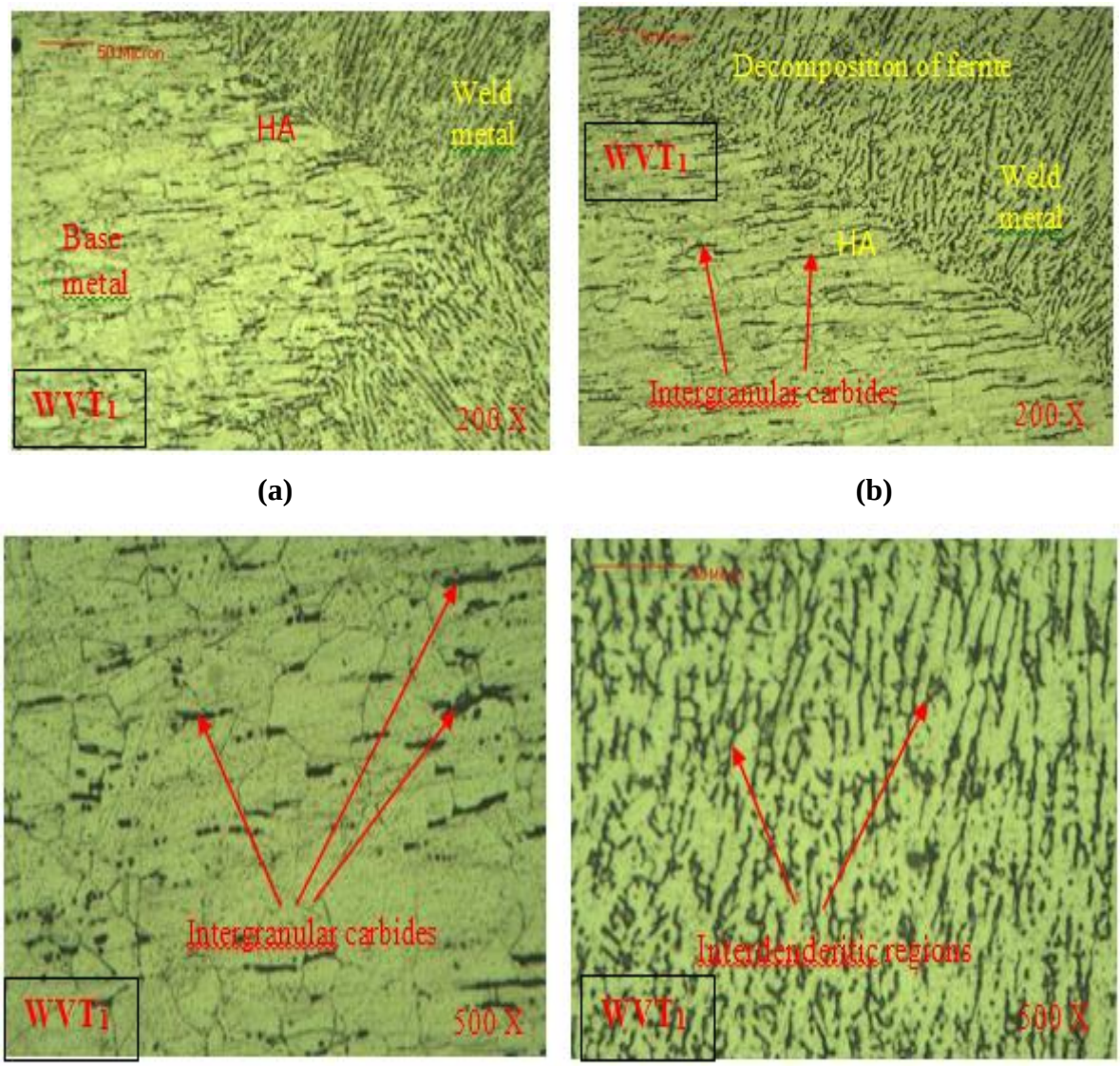

(a) **(b)**

(c) **(d)**

(a)Microstructure showing carbide precipitation in base metal, HAZ and weld metal region

(b)Microstructure showing decomposition of delta-ferrite in weld metal

(c) **Microstructure showing the inter- granular carbides at the boundaries of austenite grains in specimen WVT1**

(d) **Microstructure of weld metal showing interdendritic regions and decomposition of ferrite inspecimen WVT1**

Figure 4.3. Photomicrographs of Single-V submerged arc AISI 316L welds after thermal aging at 750 °C/24 hours

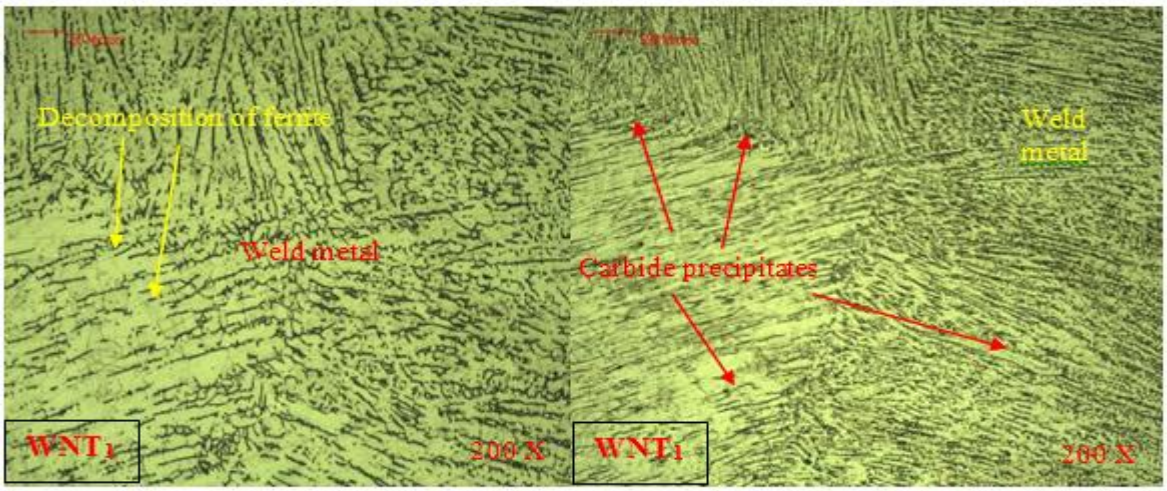

Figure 4.4. Photomicrographs of Narrow gap submerged arc AISI 316L welds after PWTA of 750°C/24 hours (a) Microstructure of specimen WNT1 showing decomposition of δ-ferrite and interdendritic carbides in weld metal (b) Composite zone showing intergranular carbides and interdendritic carbide precipitation.

Figure 4.3 showed the photomicrographs taken from different regions of specimen WVT1 (after thermal aging at 750°C/24 hours). Figure 4.3(a) shows the decomposition of δ-ferrite in weld metal and intergranular carbides in base metal and HAZ. Figure 4.8(b) shows photomicrograph taken at 500X which clearly shows the intergranular carbides formed around the austenite grains in the base metal and the HAZ region. Figure 4.8(c) displays the interdendritic regions i.e. the regions where carbide precipitation could occur and these could be the preferential sites for corrosion attack.

Figure 4.4(a)and(b)showedthephotomicrographsofnarrowgapsubmergedarcAISI316L welds after PWTA of 750°C/24 hours. Microstructural changes in the as welded and aged conditions suggested that carbide precipitations are dependent significantly upon both the temperature and time of exposure of the welds.

4.2.3 Ferrite content measurement

Tables 4.3 and 4.4 enlisted the ferrite content measurements for Single V-butt weld and narrow gap butt weld in the as deposited and aged (750℃/24 hrs.) conditions. In the as welded condition, single V-butt weld have higher ferrite content in contrast to narrow gap weld. Further, at aged condition the ferrite content was observed to be lower in welds with different joint designs which was mainly attributed to thermal active decomposition of delta ferrite into second phase particles such as carbide precipitates. The narrow gap weld

possessed relatively lower ferrite content as compared to single V-weld depicting lower availability of ferrite content for transformation to precipitates especially at aged condition.

Table 4.3. Ferrite content measurement of specimens extracted from Single-V groove butt weld in the as- welded and after different PWTA treatments (HV0.5).

PWTA treatments			Single-V weld		
Temperature (°C)	**Time (hours)**	**Specimen code**	**Weld top surface (weld pass 1)**	**Weld center**	**Weld bottom surface (weld pass 2)**
As-welded		WVT0	6.9	5.5	6.8
750	24	WVT1	4.2	3.8	4.1

Table 4.4. Ferrite content measurement of specimens extracted from Narrow gap butt weld in the as- welded and after different PWTA treatments (HV0.5).

PWTA treatments			Narrow gap weld		
Temperature (°C)	**Time (hours)**	**Specimen code**	**Weld top surface (weld pass 1)**	**Weld center**	**Weld bottom surface (weld pass 2)**
As-welded		WNT0	5.8	4.3	5.7
750	24	WNT1	3.6	2.9	3.4

4.3 Pitting Corrosion Studies

Pitting Corrosion Testing Results of Submerged Arc AISI 316l Welds

Pitting corrosion testing was carried out to study the corrosion behavior of AISI 316L welds. Specimens in the as-welded as well as after PWTA treatments were subjected to pitting corrosion testing and potentiodynamic polarization curves were generated with help of potentiostat coupled with the dedicated software. Potentiodynamic polarization curves in the as welded and thermally aged conditions for welds fabricated using different joint designs of single V-weld and Narrow gap weld are shown in Figures 4.5 and 4.6. The value of pitting potential (Epit) was measured from polarization curves and these are also shown with respective figures and was taken as a measure of pitting corrosion resistance i.e. higher the Epit value higher is the pitting resistance. Figures 4.5 and 4.6 show the comparison between polarization curves for Single-V weld and Narrow gap weld under different aged conditions. A tunaged and aged conditions, narrow gap weld exhibited a higher pitting potential as

compared to single V-weld owing to its skeletal and lacy morphological structure in the weld metal matrix. On the other hand, single V-weld possessed complete skeletal morphology which is more prone to precipitation. Due to increase in precipitation in single V-weld, pit initiation sites were also relatively higher in contrast to narrow gap weld resulting into lower pitting potential for single V-weld.

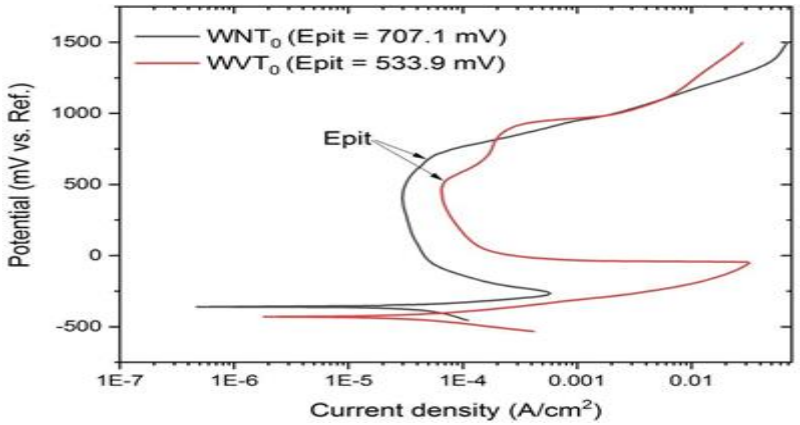

Figure 4.5.Potentiodynamic polarization curves (PPC) for welds fabricated using different joint designs in the as welded condition.

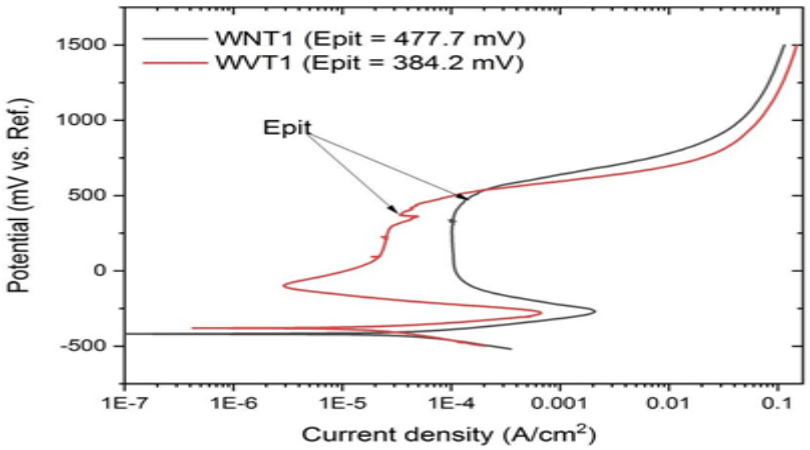

Figure 4.6. Potentiodynamic polarization curves (PPC) for welds fabricated using different joint designs at aged conditions.

4. 4 Fatigue crack growth rate studies

Figures 4.7 and 4.8 presented the fatigue crack growth rate curves of cycles count (N) vs. crack length (a mm) for single V-weld and narrow gap weld in the as welded and aged (750℃/24h) conditions. The narrow gap weld possessed relatively higher cycles count under unaged and aged conditions than single V-weld which was mainly attributed to lesser precipitation effects as observed by optical microscopy and ferrite content results. Owing to complete skeletal morphology in single V-weld, it is more prone to coarser precipitates and higher ferrite content in single V-weld leads to larger transformation delta ferrite content in

welds to second phase particles such as carbide precipitates. On the other hand, narrow gap weld exhibited much higher cycles count as compared to single V-weld due to lesser amount of precipitation and partial skeletal and lacy morphology. The results were further validated with fatigue crack growth rate curves of backpropagation ratevs.stress intensity factor (Figures4.9and 4.10) wherecrack propagation rates for both weld joint designs were plotted with reference to ASME 316L reference curve. The crack propagation rate for narrow gap weld was lower as compared to single V-weld under different aging conditions.

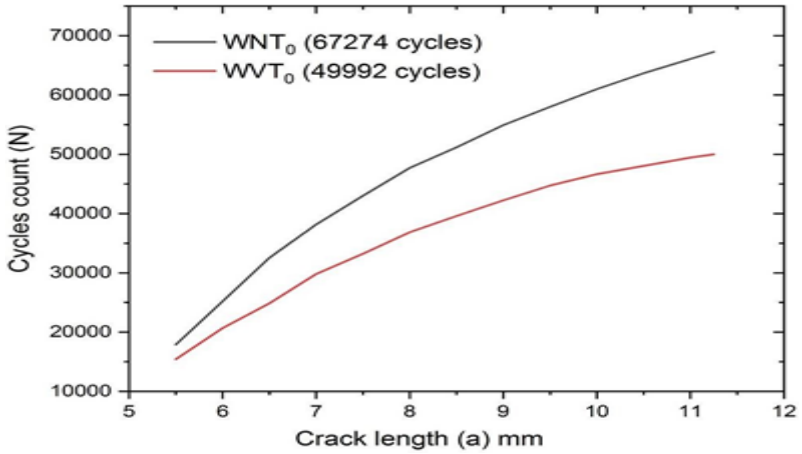

Figure 4.7.Fatigue crack growth rate (FCGR) curves (cycles count (N) vs. crack length (a mm)) for welds fabricated using different joint designs in the as welded condition.

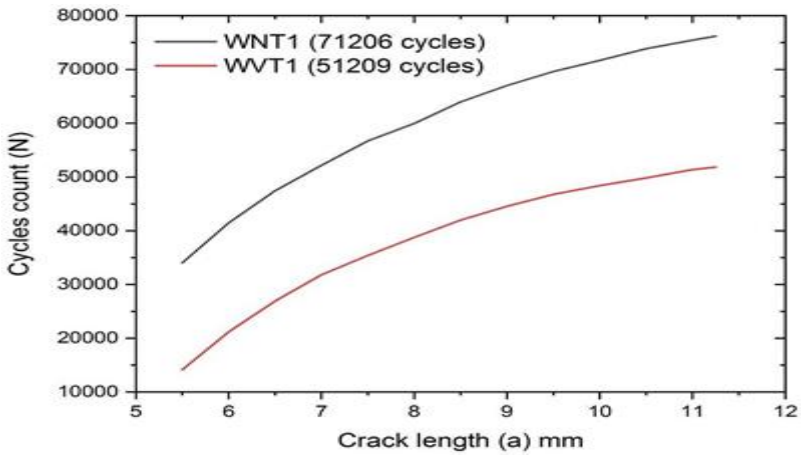

Figure 4.8. Fatigue crack growth rate (FCGR) curves (cycles count (N) vs. crack length (a mm)) for welds fabricated using different joint designs at aged condition.

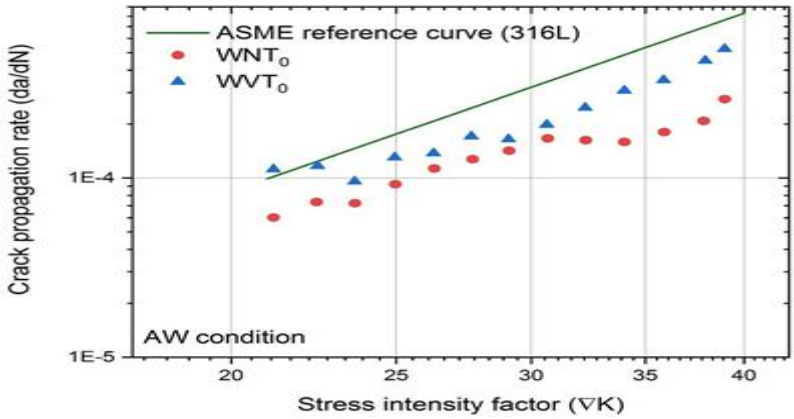

Figure 4.9. Fatigue crack growth rate (FCGR) curves (crack propagation rate (da/dN) vs. stress intensity factor for welds fabricated using different joint designs in the as welded condition.

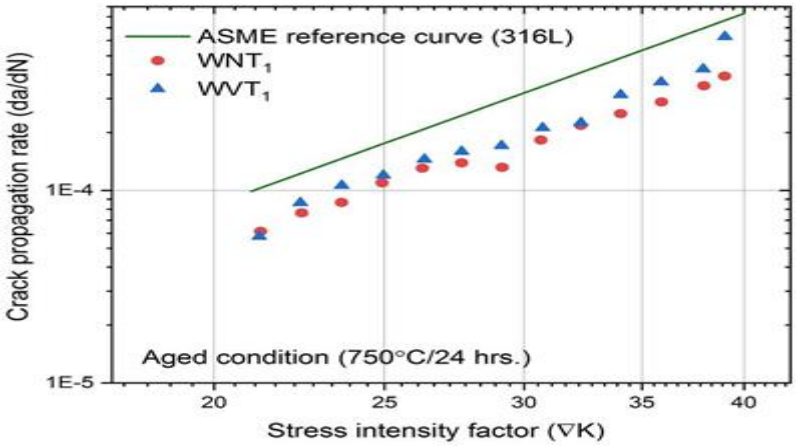

Figure 4.10. Fatigue crack growth rate (FCGR) curves (crack propagation rate (da/dN) vs. stress intensity factor for welds fabricated using different joint designs at aged condition.

CHAPTER 5

CONCLUSIONS AND FUTURE SCOPE OF WORK

5.1 Conclusions

Based upon the material combination, welding process, process parameters, procedures, and the thermal aging conditions used in this work the following main conclusions were drawn:-

1.Microhardness studies of the AISI 316L joints show that Narrow gap welds possessed relatively higher average microhardness as compared to the Single-V groove welds indicating that joint variation significantly affected the joint's cooling rate i.e. Narrow gap weld experienced higher cooling rate and hence possessed higher hardness as compared to the Single-Vweld.

2.Microstructural studies show that the weld metal of the Narrow gap joint possessed fine dendritic microstructure with partially skeletal and lathy morphology of delta ferrite as compared to the Single-V weld which possessed ferrite with skeletal morphology. Such a microstructural variation show that narrow gap welds showed relatively higher heat dissipation characteristics and hence higher cooling rate.

3.Optical microscopy revealed the decomposition of delta ferrite in the weld metal at high temperature aged condition (750 ℃/24hour).

4. Pitting studies of the welds carried out using PAP (potentiodynamic anodic polarization) technique show that narrow gap welds showed better pitting performance as compared to the single-V weld. Thermal aging of all the welds decreased their pitting resistance as revealed by the respective Epit values exhibited by them. The maximum loss of pitting resistance of the welds was observed for the aging condition of 750℃/24hour.

5.Aging condition of 750℃/24 hour resulted into inducing carbide precipitation and ferrite decomposition in the weld to such an extent that the FCGR performance of the weld metal of both single V and narrow gap butt joints were found to be higher as compared to as deposited condition. The crack propagation rates in welds at aged condition was lower relative to unaged welds owing to formation of carbide precipitates in welds.

6.The present study show that correlations existed among these AISI 316L welds in a way that ferrite morphology of the weld metal and carbide precipitation influenced their pitting behavior significantly which further influenced their FCGR performance. Thus this study reveals that Narrow gap welds are better suited for pitting environments whereas Single-V welds are more suited for fatigue applications.

5.2 Future Scope of work

1.Carbide precipitation behavior of AISI 316L welds and its composition can be further studied using material characterization techniques like SEM (Scanning Electron Microscope) with EDS (Energy dispersive X-ray spectroscopy) and TEM (Transmission electron microscopy).

2.Post weld thermal aging treatments comprising of long term exposures can further help in studying the corrosion behavior of precipitated welds.

3.Using other processes like laser and electron beam welding, comparative studies can be carried out to study the influence of process variation on the corrosion and FCGR performance of these welds.

REFERENCES

1.V. Moura, Y.A. Kina, S.S.M. Tavares, "Investigation of cracks and sensitization in an AISI 304L stainless steel exposed to 500-600 ℃." Elsevier, Engineering Failure Analysis 16 (2009)545-551.

2.M. Dadfar, M.H. Fathi, F. Karimzadeh, M.R. Dadfar, " Effect of TIG welding on corrosion behavior of 316L stainless steel." Elsevier, Materials Letters 61 (2007) 2343- 2346.

3.M.G. Pujar, R.K. Dayal, T.P.S. Gill, S.N. Malhotra, Journal of Materials Science Letters 18 (1999)823.

4.F. Liu, Y.H. Hwang, S.W. Nam, "Precipitation of σ-phase and creep-fatigue behavior of 308L steel weldment." Elsevier, Materials Science and Engineering A 483-484 (2008) 418-421.

5.U. KamachiMudali, T.P.S. Gill, R.K. Dayal and J.B. Gnanamoorthy, "Influence of nitrogen addition on microstructure and pitting corrosion resistance of austenitic weld metals". Iron and Steel Institute of Japan International, 36 (1996), pp.799-806.

6.Rahul Unnikrishnan, K.S.N SatishIdury, Sanjay G. Sapate, "Effect of heat input on the microstructure, residual stresses and corrosion resistance of 304L austenitic stainless steel weldments". Elsevier, Materials Characterization 93 (2014)10-23.

7.N. Parvathavarthini, R.K. Dayal, "Influence of chemical composition, prior deformation and prolonged thermal aging on the sensitization characteristics of austenitic stainless steels." Elsevier, Journal of Nuclear Materials 305 (2002)209-219.

8.T.P.S. Gill, J.B. Gnanamoorthy and K.A. Padmanabhan, Corrosion, 43 (1987), p.104.

9.MohdWarikhAbd Rashid, MironGakim, ZulkifiMohdRosli, "Formation of Cr23C6 during the Sensitization of AISI 304 Stainless Steel and its effect to Pitting Resistance." International Journal of Electrochemical Science, 7 (2012)9465-9477.

10. CleitonCarvalho Silva, Jesualdo Pereira Farias, "Evaluation of AISI 316L stainless steel welded plates in heavy petroleum environment." Elsevier, Materials and Design 30 (2009)1581-1587.

11.S. Ningshen, P. Shankar, K. Sanjay Rai and R.K. Dayal, Proceedings of the International Symposium on Electrochemical Methods in Corrosion Research (EMCR 2000), Budapest (Hungary), 2000, paper no.125.

12.S.A. Tukur, M.S. Dambatta, A, Ahmed, N.M. Mu'az, "Effect of Heat Treatment on mechanical properties of AISI 304 Stainless Steel." International journal of Innovative Research in Science, Engineering and Technology, Vol. 3, Issue 2,2014.

13.C. Gracia, M.P. de Tiedra, Y. blanco, O. Martin, “Intergranular corrosion of welded joints of austenitic stainless steels studied by using an electrochemical minicell.” Elsevier, Corrosion Science 50 (2008)2390-2397.

14.A.I. Grekula, V.P. Kujanpaa and L.P. Karjalainen, Corrosion 40 (1984)569.

15.L. Li, C.F. Dong, K. Xiao, J.Z. Yao and X.G. Li, “Effect of pH on pitting corrosion of stainless steel welds in alkaline salt water.” Construction and Building Materials 68 (2014)709–715.

16.Subodh Kumar, A.S. Shahi, “Studies on metallurgical and impact toughness behavior of variably sensitized weld metal and heat affected zone of AISI 304L welds.” Elsevier, Materials and Design 89 (2016)399-412.

17.L.A. James, “Crack Propagation Behavior in type 304 Stainless Steel weldments at Elevated Temperature.” Welding Research Supplement, April,1973.

18.K. Chandra, VivekanandKain, VikasBhutani, V.S. Raja, R. Tewari, “Low temperature thermal aging of austenitic stainless steel welds: Kinetics and effect on mechanical properties.” Elsevier, Materials Science and Engineering A 534 (2012)163-175.

19.MáriaDománková, Edina Kocsisová, Ivan Slatkovský, Peter Pinke, “The Microstructure Evolution and Its Effect on Corrosion Properties of 18Cr-12Ni-2,5Mo Steel Annealed at 500-900°C.” ActaPolytechnicaHungarica, Vol. 11, Nov. 3,2014.

20.Ayo Afolabi and NajeemPeleowo, “Effect of Heat Treatment on Corrosion Behavior of Austenitic Stainless Steel in Mild Acid Medium.” International Conference on Chemical, Ecology and Environmental Sciences (ICCEES'2011) Pattaya Dec.2011.

21.H. Sahlaoui, K. Makhlouf, H. Sidhoma and J. Philibert, “Effects of ageing conditions on theprecipitatesevolution,chromiumdepletionandintergranularcorrosionsusceptibilityof AISI 316L: experimental and modeling results.” Elsevier, Materials Science and Engineering A 372 (2004) 98–108.

22.C.S. Kusko, J.N. Dupont and A,R. Marder, “The Influence of microstructure on Fatigue Crack Propagation behavior of Stainless Steel welds.” Welding Research, January,2004.

23.J.J. Coronado and C. Ceron, “Fracture mechanisms of CTOD samples of submerged and flux cored arc welding.” Elsevier, Theoretical and Applied Fracture Mechanics 53 (2010) 145-151.

24.Jong-Hyun Baek, Woo-Sik Kim and Young-Tai Kho, “Fracture toughness and fatigue crack growth properties of the base metal and weld metal of the type 304 stainless steel pipeline for LNG transmission.” Elsevier, International Journal of Pressure Vessels and Piping 78 (2008)351-357.